



ELSEVIER

Journal of Crystal Growth 243 (2002) 546–560

JOURNAL OF
**CRYSTAL
GROWTH**

www.elsevier.com/locate/jcrysgr

Approximate material-balance solution to the moving meniscus model of detached solidification

Yazhen Wang¹, Liya L. Regel*, William R. Wilcox

International Center for Gravity Materials Science and Applications, Clarkson University, Box 5814, Potsdam, NY 13699-5814, USA

Received 4 December 2001; accepted 18 June 2002

Communicated by R.S. Feigelson

Abstract

Non-dimensionalization of the governing equations for the Moving Meniscus Model of detached solidification in zero gravity allowed consolidation of the operating conditions and physical properties into 5 dimensionless parameters: a dimensionless meniscus factor, a freezing rate Peclet number, the interfacial segregation coefficient k for dissolved gas, the ratio of gas solubility at the end of the melt to that at the meniscus, and the ratio of gas concentration in the gap to that in the adjacent melt. At steady state, the flux of gas dissolved in the melt moving toward the freezing interface must equal the sum of the flux of gas into the gap plus that being incorporated in the growing solid. Both numerical and material-balance results give two solutions, with an extremum value of each variable beyond which steady detachment is impossible. This behavior is now understood to originate from satisfaction of the material balance at two different gap widths, with these two solutions becoming identical at an extremum condition beyond which the material balance cannot be satisfied. Only one solution is obtained when no gas is incorporated in the solid. In the presence of gravity, the gas pressure in the gap must be much larger to compensate for the added hydrostatic pressure, causing the gap width to be narrow.

© 2002 Elsevier Science B.V. All rights reserved.

PACS: 64.70.D; 64.75; 81.10.F; 81.80

Keywords: A1. Directional solidification; A1. Mass transfer; A2. Bridgman technique; A2. Gradient freeze technique; A2. Microgravity conditions; B2. Semiconducting indium compounds

1. Introduction

Many directional solidification experiments in space yielded ingots with sections that had little or no contact with the ampoule wall [reviewed in Ref. 1]. We call this “detached solidification”. When

*Corresponding author. Fax: +1-315-268-3833.

E-mail address: regel@clarkson.edu (L.L. Regel).

¹Current address: Chemistry Department, Vanderbilt University, Nashville, TN 37240, USA.

Nomenclature

The numerical values given in parentheses are the base values used in the examples, and are intended to simulate solidification of InSb.

a	acceleration (9.8 m/s^2)
A_1, A_2	constants in Eq. (14)
B_1, B_2	constants in Eq. (17)
C	concentration of gas dissolved in the melt (mol/m^3)
C_0	concentration of dissolved gas in the melt at the freezing interface (mol/m^3)
C_∞	concentration of dissolved gas far from the freezing interface (mol/m^3)
C_g	concentration of dissolved gas in the melt at the meniscus (mol/m^3)
C_{gap}	concentration of gas in the gap, RT_g/P_g (mol/m^3)
D	diffusion coefficient in the melt ($1 \times 10^{-9} \text{ m}^2/\text{s}$)
e	gap width (m)
f	a function depending only on x^*
g	a function depending only on r^*
h	height of the melt above the freezing interface (0.05 m)
H_m	Henry's law constant at the top of the melt, C_∞/P_m ($0.00016 \text{ mol/m}^3 \text{ Pa}$)
H_g	Henry's law constant at the meniscus, C_g/P_g ($0.00013 \text{ mol/m}^3 \text{ Pa}$)
$J_n(z)$	Bessel function of the first kind of variable z and order n
L	distance from the freezing interface into the melt, beyond which the velocity and the dissolved gas concentration are constant (m)
N_G	gas flux into the gap through the meniscus (mol/s)
N_L	gas flux in with the melt at L (mol/s)
N_L^0	gas flux in with the melt without detachment (mol/s)
N_S	gas flux into the solid at the freezing interface (mol/s)
P_m	gas pressure above the melt (100 Pa)
P_g	gas pressure in the gap (Pa)
R	ideal gas constant ($8.314 \text{ m}^3 \text{ Pa/mol K}$)
r	radial distance from the ampoule's axis (m)
r_a	ampoule radius (0.01 m)
T_g	average temperature of the gas in the gap (800 K)
V_c	freezing rate ($1 \times 10^{-6} \text{ m/s}$)
V_x	velocity of the melt in the axial direction (m/s)
V_r	velocity of the melt in the radial direction (m/s)
x	axial distance from the freezing interface (m)
$Y_n(z)$	Bessel function of the second kind of variable z and order n . Also called Weber's function

Greek letters

α	growth angle (see Fig. 1) (25°)
λ	constant resulting from separation of variables in differential equation for concentration, Eqs. (12) and (13)
θ	contact angle for the melt on the ampoule wall (see Fig. 1) (112°)
ρ	density of the melt (6430 kg/m^3)
σ	surface tension between the melt and the gas phase (0.43 N/m)

Dimensionless parameters

C^*	dimensionless concentration of dissolved gas in the melt, C/C_∞
C_m^*	dimensionless concentration of dissolved gas at the meniscus, C_g/C_∞
C_0^*	dimensionless concentration of dissolved gas at the freezing interface, C_0/C_∞
k	segregation or distribution coefficient; ratio of the concentration of gas incorporated in the growing crystal to that in the adjacent melt (0.03).
N_S^*	dimensionless gas flux into the solid, N_S/N_L^0
N_G^*	dimensionless gas flux into the gap, N_G/N_L^0
N_L^*	dimensionless gas flux in with the melt, N_L/N_L^0
Pe	dimensionless freezing rate Peclet number, $V_c r_a / D$ (10)
r^*	dimensionless radial distance, r/r_a
V_x^*	dimensionless velocity in the axial direction, $V_x r_a / D$
V_r^*	dimensionless velocity in the radial direction, $V_r r_a / D$
x^*	dimensionless axial distance, x/r_a
β	ratio of Henry's law constants in gap and at the end of the melt, H_g/H_m (0.8125)
Γ	dimensionless hydrostatic pressure, $\rho a h / P_m$ (31.51)
κ	melt surface parameter, $-\sigma \cos \theta / r_a P_m$ (0.1611)
χ	ratio of gas concentration in the gap to that dissolved in the melt adjacent to the meniscus, $1/RT_g H_g = C_{\text{gap}}/C_g$ (1.157)
ε	dimensionless gap width, e/r_a
η	meniscus factor, $\sigma(\cos \theta + \cos \alpha) / r_a P_m$ (0.2286)
Π	dimensionless pressure change between the top surface of the melt and the gap, $(P_g - P_m)/P_m$

detachment occurs, the dislocation density is greatly reduced and grains and twins can no longer nucleate at the ampoule wall. Regel and Wilcox [2] proposed the Moving Meniscus Model shown in Fig. 1 to explain this puzzling phenomenon. There is a gap between the solid and the ampoule wall, while the melt remains in contact with the ampoule. During solidification, the meniscus moves along the ampoule wall at the freezing rate. There must be a pressure difference across the meniscus because of its curvature. This pressure difference is provided by a gas, which is dissolved in the melt at its top surface, rejected by the growing solid, and released across the meniscus into the gap. Based on the Moving Meniscus Model, numerical calculations were performed for InSb [3–6] and for water [7]. Detached solidification was predicted to occur in a sealed ampoule at zero gravity under proper conditions; the gas pressure P_m above the melt must be above a critical value [3,7], the freezing rate V_c must exceed a critical value [3,7], Henry's constant H of the dissolved gas must be below a critical value [7], the temperature of the top of the melt must be below a critical value [7], the contact angle θ of the melt on the ampoule wall and the growth angle α must exceed critical values [4], and the diffusion coefficient D of the gas in the melt must exceed a critical value [3,7].² Each critical value depends on the other physical properties and operating conditions, so that different results were obtained for InSb and water [7]. Within the range of parameters predicted to yield steady-state detachment, two solutions were found, one with a large gap and one with a small gap between the solid and the ampoule wall.

As is typical of numerical simulations, a thorough understanding of the factors contributing to the behavior predicted above has been elusive. For that reason we sought to develop an approximate analytical

²See Fig. 1 for the meanings of θ and α . Symbols are also defined in the table of Nomenclature, along with the values of the parameters for the InSb base case used here to illustrate detached behavior.

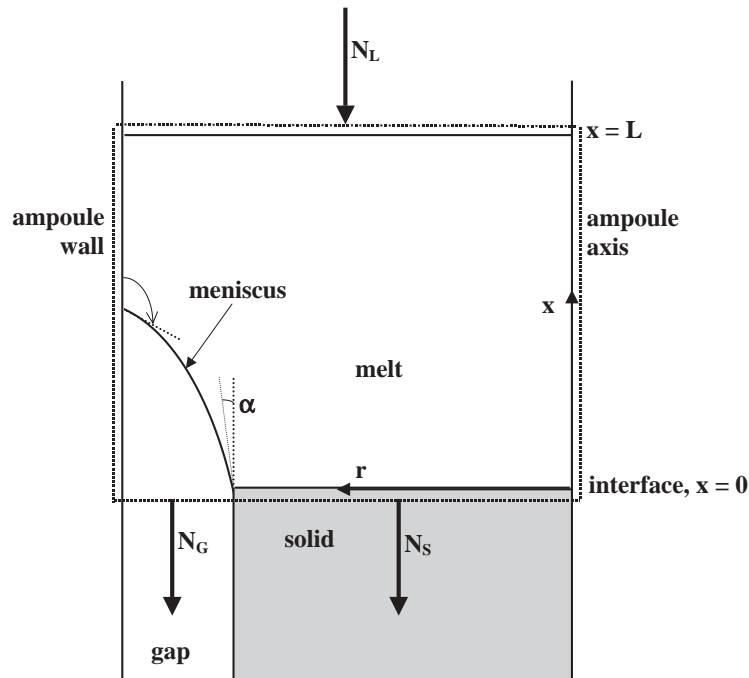


Fig. 1. Schematic diagram of detached solidification. The dotted line shows the cylindrical material-balance surface. Symbols are defined in the Nomenclature.

solution. We were encouraged by the observation that although Marangoni convection along the meniscus dramatically alters the computed velocity and concentration fields, it does not markedly influence detachment [3]. The steady-state material-balance approach described below was successful, and does reveal the essential physics.

2. Fluxes of residual gas

In order to perform a steady-state material balance, one first defines the material-balance domain, then estimates the fluxes into and out of the domain, and finally sets the total flux to zero. Here, we focus on the fluxes of a residual gas that dissolves in the melt. We define the cylindrical material-balance domain shown as the dotted line in Fig. 1. It moves along with the freezing interface at freezing rate V_c and is bounded by the ampoule wall, a cross-sectional plane just inside the solid, and another plane in the melt at distance L from the freezing interface. At steady state, the molar gas flux N_L into the domain with the melt at L must equal that into the gap, N_G , plus that into the growing solid, N_S . Note that each flux (in mol/s) is the product of the volumetric flow rate (in m^3/s) through the domain boundary and the molar concentration (in mol/m^3) there. Below, we estimate these fluxes and then use them to determine the influence of the properties and operating parameters on detachment. It is assumed that there is no convective mixing in the melt, that the growth material is pure except for a dissolved gas present at low concentration, and that the density of the melt is constant and equal to that of the solid. The strict validity of these assumptions is not necessary for the basic physics to be revealed.

2.1. Flux into the material-balance surface

The sole flux into the material-balance domain is that entering with the melt at L . The total volumetric flow of melt entering the domain at L is equal to that leaving into the freezing solid, which is the cross-sectional area of the growth interface times the growth velocity. The flux of dissolved gas at $x = L$ is the product of this volumetric flow rate and its concentration there, $C_\infty = H_m P_m$.³

In the absence of a gap, the volumetric flow into the solid is $\pi r_a^2 V_c$ and so the gas flux at L is

$$N_L^0 = \pi r_a^2 V_c C_\infty = \pi r_a^2 V_c H_m P_m, \quad (1)$$

where the superscript 0 denotes the value at zero gap width ($e = 0$). We will use this flux to non-dimensionalize each of the three fluxes.

With a finite gap width, the volumetric flow rate of melt into the domain at L is reduced by the diminished cross-sectional area of the growing solid, while the concentration of dissolved gas remains the same. Thus

$$N_L^* \equiv \frac{N_L}{N_L^0} = (1 - \varepsilon)^2, \quad (2)$$

where the asterisk denotes a dimensionless flux, and $\varepsilon \equiv e/r_a$ is the dimensionless gap width. Note that this equation is exact so long as there is no convective mixing across the surface $x = L$, and is approximately linear in ε for small values of gap width.

2.2. Flux out of the material-balance surface into the gap

The flux into the gap, N_G , is equal to the rate of increase of gap volume times the molar density, which depends on the pressure in the gap, P_g . Duffar et al. [8] derived the relationship between this pressure, that at the top of the melt (P_m), and the factors determining the curvatures of the meniscus and the end of the melt at zero gravity. Using geometric conditions at zero gravity, they found expressions for these curvatures, which depend on the ampoule radius r_a , the contact angle θ of the melt on the ampoule wall, and the growth angle α , but not on the melt–gas surface tension σ . The pressure difference across such a surface is the product of σ and the curvature, i.e. the Laplace equation. The result of Duffar et al. [8] is given in their Eq. (12) as a solution for the gap width e . We obtain⁴ from this equation the following:

$$P_g - P_m = \frac{2\sigma r_a (r_a - e)(\cos \theta + \cos \alpha)}{e r_a (2r_a - e)} - \frac{2\sigma e (r_a - e) \cos \theta}{e r_a (2r_a - e)}. \quad (3)$$

Here, the first term is the pressure change across the meniscus and the second term is the pressure change across the top surface of the melt. Adding the term $\rho a h$ for the hydrostatic pressure and non-dimensionalizing we obtain

$$\Pi \equiv \frac{P_g - P_m}{P_m} = \frac{2 - 2\varepsilon \eta}{2 - \varepsilon} \frac{\eta}{\varepsilon} + \frac{2 - 2\varepsilon}{2 - \varepsilon} \kappa + \Gamma, \quad (4)$$

where $\eta \equiv \sigma(\cos \theta + \cos \alpha)/r_a P_m$ is the dimensionless meniscus parameter, $\kappa \equiv -\sigma \cos \theta/r_a P_m$ is the dimensionless melt surface parameter, and $\Gamma \equiv \rho a h/P_m$ is the dimensionless hydrostatic pressure.⁵ A value of $\eta = 0$ corresponds to a flat meniscus with no curvature, which occurs when $\theta + \alpha = \pi$ (180°) and is the special case addressed by Duffar [8] for an ampoule open at both ends. As the sum of these angles

³ The value of L is taken to be sufficiently large that this concentration equals that at the top melt surface, which is in equilibrium with the gas at pressure P_m , or $C_\infty = H_m P_m$ from the definition of the Henry's law constant, H_m .

⁴ The algebraic manipulations and most of the plotting were carried out using the computer algebra system Maple (<http://www.maplesoft.com/>).

⁵ In our previous papers [3–7], we used the limiting case of $\varepsilon \rightarrow 0$, or $\Pi = \eta/\varepsilon$.

decreases, η increases, the meniscus becomes more curved, and detachment becomes more difficult (as shown later). The term η/ε in Eq. (4) gives the pressure increase due to the curvature of the meniscus when the gap width is much less than the ampoule radius ($\varepsilon \ll 1$), and κ gives the pressure increase⁶ due to the curvature of the top melt surface. The factor $(2 - 2\varepsilon)/(2 - \varepsilon)$ corrects for the influence of finite ampoule radius on the meniscus curvature. The pressure increase due to hydrostatic pressure predominates on earth except for very small gap widths, where the pressure increase across the meniscus becomes largest. The pressure in the gap approaches infinity in the limit of zero gap width when $\theta + \alpha < \pi$.

We assume the gas in the gap obeys the ideal-gas law and that its average temperature T_g remains constant, so that its concentration is P_g/RT_g . The volumetric flow of gas is the cross-sectional area of the gap times the growth rate. Thus the flux into the gap is

$$N_G = \frac{\pi(r_a^2 - (r_a - e)^2)V_c P_g}{RT_g} \tag{5}$$

Substituting for P_g from Eq. (4) and dividing by Eq. (1) we obtain the desired expression for dimensionless flux into the gap

$$N_G^* \equiv \frac{N_G}{N_L^0} = [\varepsilon(2 - \varepsilon) + 2\eta(1 - \varepsilon) + 2\kappa\varepsilon(1 - \varepsilon) + \Gamma\varepsilon(2 - \varepsilon)]\chi\beta, \tag{6}$$

where $\chi \equiv 1/RT_g H_g = C_{\text{gap}}/C_g$ is the ratio of gas concentration in the gap to that dissolved in the melt adjacent to the meniscus, and $\beta \equiv H_g/H_m$ is the ratio of Henry's law constants at the meniscus and at the top end of the melt.⁷ For the base parameters, the flux into the gap at zero gravity increases almost linearly with gap width, and approaches a finite value for zero gap width.⁸ This finite limiting value reflects the fact that for $\eta > 0$ the pressure in the gap approaches infinity as $\varepsilon \rightarrow 0$.

2.3. Flux of dissolved gas out of the material-balance surface into the growing solid

As above, the flux N_S equals the volumetric flow rate times the concentration in the solid, kC_0 , where C_0 is the concentration of dissolved gas in the adjacent melt. Since C_0 is a function of radial position r we must integrate over the freezing interface to obtain

$$N_S = V_c k \int_0^{r_a - e} 2\pi r C_0 \, dr = 2\pi V_c k C_\infty \int_0^{1 - \varepsilon} r^* C_0^* \, dr^*, \tag{7}$$

where the second expression is in dimensionless form with $r^* \equiv r/r_a$ and $C_0^* \equiv C_0/C_\infty$. In order to estimate the radial dependence of interfacial concentration, we begin with the differential equation for mass transfer in the melt

$$V_r^* \frac{\partial C^*}{\partial r^*} + V_x^* \frac{\partial C^*}{\partial x^*} = \frac{1}{r^*} \frac{\partial}{\partial r^*} \left(r^* \frac{\partial C^*}{\partial r^*} \right) + \frac{\partial^2 C^*}{\partial x^{*2}}, \tag{8}$$

where $V_x^* \equiv -V_x r_a/D$ is the dimensionless melt velocity in the axial direction (away from the freezing interface), $V_r^* \equiv -V_r r_a/D$ is the dimensionless melt velocity in the radial direction, and $C^* \equiv C/C_\infty$ is the dimensionless gas concentration in the melt at any position.

We assume that near the freezing interface we can approximate the concentration field as the product of a function f depending only on axial position and another function g depending only on radial position, i.e.

⁶Pressure increase for $\cos \theta < 0$, i.e. $\theta > 90^\circ$.

⁷Unfortunately, we have been unable to find data or a method to estimate theoretically the diffusion coefficients or solubilities of gases in semiconductor melts or solids. Thus, the values of D , H_g , H_m and k used here for the InSb base case were guessed.

⁸ $\eta \leq 0$ corresponds to $\theta + \alpha \geq 180^\circ$, i.e. a meniscus of zero or negative curvature.

$C^* = f(x^*) \cdot g(r^*)$. With this assumption, Eq. (8) becomes

$$V_r^* f \frac{dg}{dr^*} + V_x^* g \frac{df}{dx^*} = f \frac{1}{r^*} \frac{d}{dr^*} \left(r^* \frac{dg}{dr^*} \right) + g \frac{d^2 f}{dx^{*2}}. \quad (9)$$

We note that at the freezing interface ($x^* = 0$), $V_r = 0$ and $V_x = -V_c$, or in dimensionless form

$$V_x^* = -\frac{V_c r_a}{D} = -Pe, \quad (10)$$

where $Pe = V_c r_a / D$ is the freezing rate Peclet number. We assume that these conditions on the melt velocity are approximately valid near the freezing interface. Substituting Eq. (10) into Eq. (9) and setting $V_r^* = 0$ we obtain

$$-Pe g \left(\frac{df}{dx^*} \right) = f \frac{1}{r^*} \frac{d}{dr^*} \left(r^* \frac{dg}{dr^*} \right) + g \left(\frac{d^2 f}{dx^{*2}} \right). \quad (11)$$

We rearrange Eq. (11) so that all of the x^* -dependent terms are on one side of the equation and all of the r^* -dependent terms are on the other side. This requires that both sides be a constant, which we represent by λ^2 . The result is an ordinary differential equation for concentration variation in the axial direction and another for the radial direction:

$$\left(\frac{d^2 f}{dx^{*2}} \right) + Pe \left(\frac{df}{dx^*} \right) - \lambda^2 f = 0, \quad (12)$$

$$\frac{1}{r^*} \frac{d}{dr^*} \left(r^* \frac{dg}{dr^*} \right) = -\lambda^2. \quad (13)$$

The solution to Eq. (12) is

$$f = A_1 \exp \left[\frac{-Pe + \sqrt{Pe^2 + 4\lambda^2}}{2} x^* \right] + A_2 \exp \left[\frac{-Pe - \sqrt{Pe^2 + 4\lambda^2}}{2} x^* \right], \quad (14)$$

where A_1 and A_2 are constants. For $x^* \rightarrow \infty$, C^* and f remain finite, so that $A_1 = 0$. At $x^* = 0$ an interfacial material balance yields

$$\frac{dC^*}{dx^*} = -Pe(1-k)C^* \quad \text{and so} \quad \left(\frac{df}{dx^*} \right) = -Pe(1-k)f, \quad (15)$$

where k is the segregation coefficient for the dissolved gas. From Eqs. (14) and (15), we get

$$\lambda = Pe \sqrt{k(1-k)}. \quad (16)$$

The solution to Eq. (13) is

$$g = B_1 J_0(\lambda r^*) + B_2 Y_0(\lambda r^*), \quad (17)$$

where J_0 and Y_0 are Bessel functions, and B_1 and B_2 are constants. On the axis ($r^* = 0$) there can be no radial flux, and so

$$\frac{dC^*}{dr^*} = 0 \quad \text{and} \quad \frac{dg}{dr^*} = 0. \quad (18)$$

Thus, $B_2 = 0$.

Combining the solutions for f and g we get

$$C^*(x^*, r^*) \equiv f(x^*)g(r^*) = A_2 B_1 J_0(\lambda r^*) \exp \left(\frac{-Pe - \sqrt{Pe^2 + 4\lambda^2}}{2} x^* \right) \quad (19)$$

with A_2B_1 still to be evaluated. At the freezing interface ($x^* = 0$), Eq. (19) becomes

$$C_0^* = A_2B_1J_0(Pe\sqrt{k(1-k)}r^*). \tag{20}$$

At the point where the freezing interface meets the meniscus, $r^* = 1 - \varepsilon$, the melt is in equilibrium with gas in the gap. The concentration C_g of dissolved gas at the meniscus is given by H_gP_g . Substituting for P_g from Eq. (4) and using the definition for β we find

$$C_g^* \equiv \frac{C_g}{C_\infty} = \frac{H_gP_g}{H_mP_m} = \beta \left[1 + \frac{2 - 2\varepsilon\eta}{2 - \varepsilon} \frac{\eta}{\varepsilon} + \frac{2 - 2\varepsilon}{2 - \varepsilon} \kappa + \Gamma \right]. \tag{21}$$

Substituting Eq. (21) into Eq. (20) with $r^* = 1 - \varepsilon$

$$A_2B_1 = \beta \frac{2(\eta + \varepsilon\kappa)(1 - \varepsilon) + \varepsilon(1 + \Gamma)(2 - \varepsilon)}{\varepsilon(2 - \varepsilon)J_0(Pe\sqrt{k(1-k)}(1 - \varepsilon))}. \tag{22}$$

Substituting Eq. (22) into Eq. (20), the result into Eq. (7), and dividing by Eq. (1), we obtain an estimate for the dimensionless flux of dissolved gas into the growing solid

$$N_S^* = 2k\beta \frac{2(\eta + \varepsilon\kappa)(1 - \varepsilon) + \varepsilon(1 + \Gamma)(2 - \varepsilon)}{\varepsilon(2 - \varepsilon)} \frac{J_1(Pe\sqrt{k(1-k)}(1 - \varepsilon))}{J_0(Pe\sqrt{k(1-k)}(1 - \varepsilon))}. \tag{23}$$

The interfacial concentration found here is compared with the results of our numerical calculations in Fig. 2. Note that the present approximation is low, and so the resulting flux into the solid must also be low. (Fig. 2 also shows the dimensionless steady-state interfacial concentration in the absence of a gap, $1/k$.) Better approximations to the numerical results could probably be devised, but only by violating one or more of the boundary conditions for the concentration field. Fortunately, the present expression varies in the proper way with the experimental variables and material properties. The flux into the solid increases with decreasing gap width. It increases to infinity as the gap width approaches zero, reflecting equilibrium at the meniscus with a pressure increasing without bound. The flux increases with increasing Peclet number because the total flow of material into the solid increases.

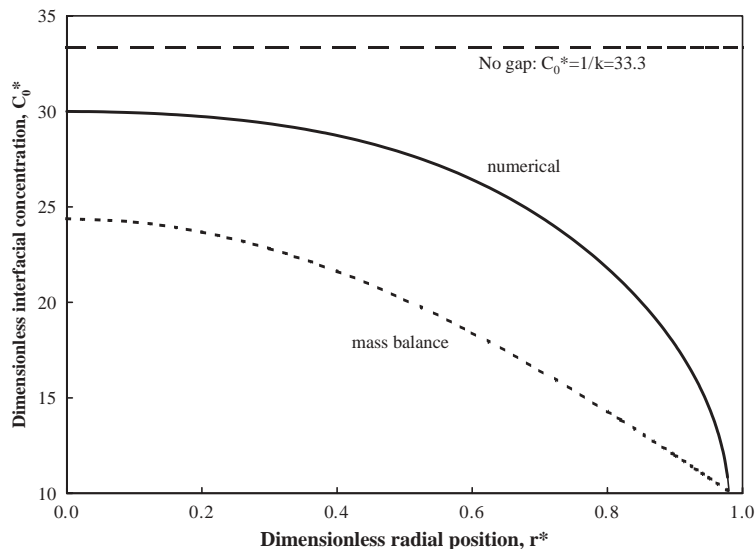


Fig. 2. Comparison of numerical and material-balance predictions from Eqs. (20) and (22) for the dimensionless concentration C_0^* along the freezing interface for a dimensionless gap width $\varepsilon = 0.02$ and values of the other parameters as given in Nomenclature.

3. Material balance

The material-balance relationship is expressed by

$$N_L^* = N_G^* + N_S^* \quad (24)$$

with the dimensionless fluxes given by Eqs. (2), (6) and (23). Although an explicit expression for gap width is not possible, Maple permits us to readily calculate numerical values and make plots. We now examine three particular cases: zero gravity, the influence of gravity, and zero solid solubility.

3.1. Material balance for zero gravity

At zero gravity $a = 0$ and there is no hydrostatic pressure, and so $\Gamma = 0$. Fig. 3 shows the three fluxes for the other base case values given in Nomenclature. This figure is key to understanding the physics of detached solidification. The arrows indicate the two points where Eq. (24) is satisfied and represent two possible values of the gap width, as found in all of our numerical solutions of the governing differential equations for fluid mechanics and mass transfer. Fig. 4 illustrates, with Pe as an example, how an extremum exists for each parameter, beyond which steady detachment is impossible. Two values of gap width are permissible for small values of Pe . As Pe is increased, the curve for $N_G^* + N_S^*$ rises and the two solutions move closer together. At the critical value of $Pe = 13.73$, this curve just touches the N_L^* line at one point—the extremum. For larger values of Pe there is no point at which a steady-state material balance can be satisfied.

How well does the material-balance prediction agree with our numerical results? As noted earlier, the present estimate of concentration along the freezing interface is low, causing the estimated flux into the solid to be low. Thus, the curve for $N_G^* + N_S^*$ in Fig. 3 is too low, and so we would expect the difference between small and large values of gap width to be greater than for the numerical solution, with the large value being significantly greater than the numerical solution. This point is illustrated in Fig. 5. The points represent numerical results obtained by varying η in four different ways: by varying η itself in non-dimensionalized equations, and by varying separately σ , P_m and θ while holding the other parameters constant in the dimensional equations. Since our non-dimensionalization is equally valid for the numerical approach, all four numerical results should have been identical. The scatter in the numerical “data”, therefore, indicates the error in the numerical method used to solve the Moving Meniscus Model.

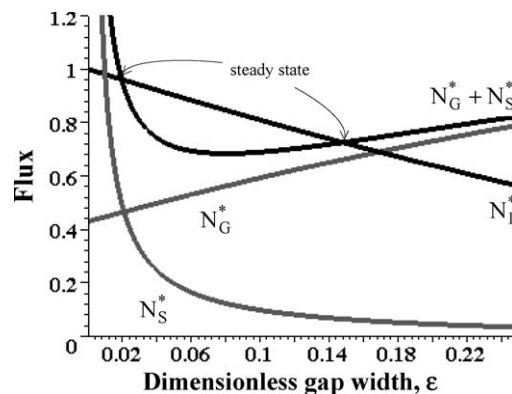


Fig. 3. Dimensionless fluxes of dissolved gas versus gap width for base conditions at zero gravity. Steady state occurs when $N_G^* + N_S^* = N_L^*$. Values of the dimensionless parameters are $k = 0.03$, $Pe = 10$, $\eta = 0.2286$, $\kappa = 0.215$, $\beta = 0.8125$, $\chi = 1.157$, $\Gamma = 0$.

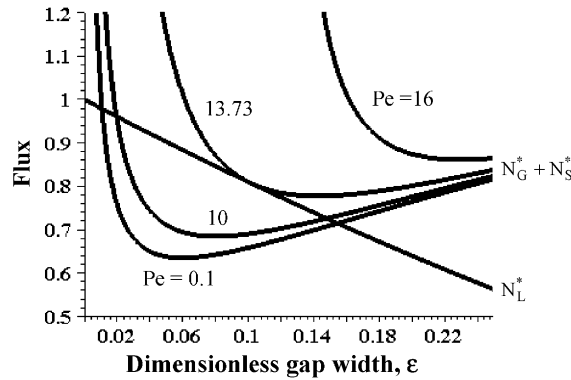


Fig. 4. Illustration of an extremum value for existence of a steady-state material balance at zero gravity. For $Pe < 13.73$ there are two steady-state solutions, at $Pe = 13.73$ one solution, and for $Pe > 13.73$ no solution. Other parameters are the base values given in Nomenclature.

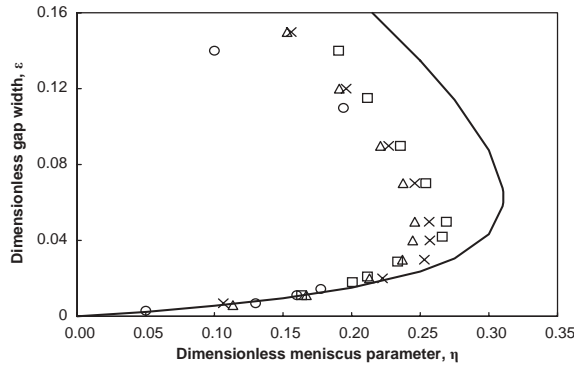


Fig. 5. Comparison of the material-balance solution with results from the numerical solution of the Moving Meniscus Model. For base parameters as given in Nomenclature, except for limiting case of very large ampoule so that $\Pi = \eta/\epsilon$. —Material balance; × numerical with σ varied; ○ numerical with η varied; □ numerical with P_m varied; △ numerical with θ varied.

Figs. 6–8 illustrate the dependence of predicted steady-state gap width on the governing dimensionless parameters. If we were to extend the range of η in Fig. 6 to negative values, we would find the curves to continue, with the small gap width becoming negative, and the large gap width still larger.

3.2. Material balance for zero flux into the solid

We now examine the limiting case of zero flux into the solid ($N_S^* = 0$), which corresponds to $k = 0$. By equating Eq. (2) to Eq. (6) and solving for the root for which $0 < \epsilon < 1$, we find

$$\epsilon = \frac{1 + \chi\beta(1 + \Gamma - \eta + \kappa) - \sqrt{\chi\beta(1 + \Gamma) + \chi^2\beta^2((1 + \Gamma)^2 + 2\kappa(1 + \Gamma) + (\eta + \kappa)^2)}}{1 + \chi\beta(1 + \Gamma + 2\kappa)} \tag{25}$$

Because our estimates for flux into the domain and into the gap are reasonably accurate, this equation is valid so long as the assumptions are obeyed fairly well. Note that in this case the gap width does not depend on the freezing rate (through the Peclet number Pe). In practice, as Pe is increased, gas bubble nucleation

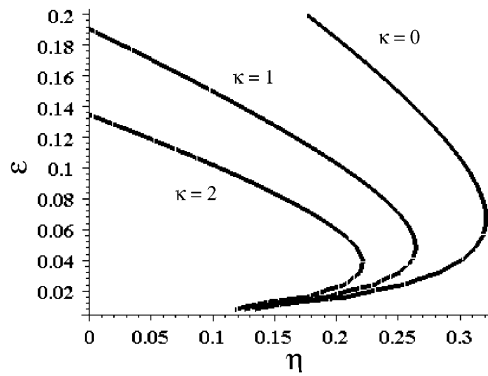


Fig. 6. Dimensionless gap width ε versus meniscus parameter η and melt surface parameter κ .

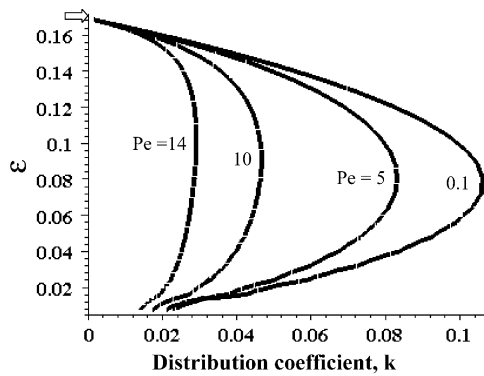


Fig. 7. Dimensionless gap width ε versus the segregation coefficient k for the dissolved gas and the freezing rate Pecllet number Pe . \Rightarrow from the solution for material balance with $N_S^* = 0$, Eq. (25).

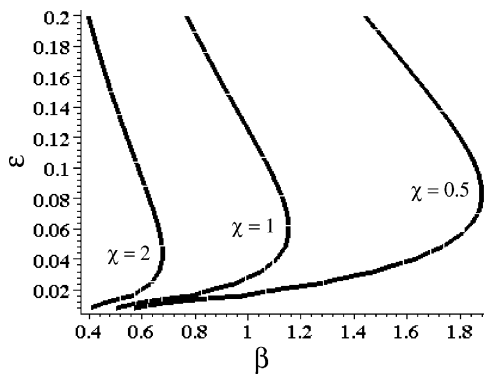


Fig. 8. Dimensionless gap width ($\varepsilon = e/r_a$) versus β (ratio of gas solubility in the gap to that at the end of the melt) and χ (ratio of gas concentration in the gap to that in the adjacent melt).

will occur near the center of the ampoule ($r \approx 0$) due to the increased gas concentration there (see, for example Ref. [9]). The gas rejected by the growing interface is no longer able to diffuse into the gap sufficiently rapidly. The open arrow in Fig. 7 shows that this limiting case corresponds approximately to an extrapolation of the branch of the curve for the larger gap width to $k = 0$.

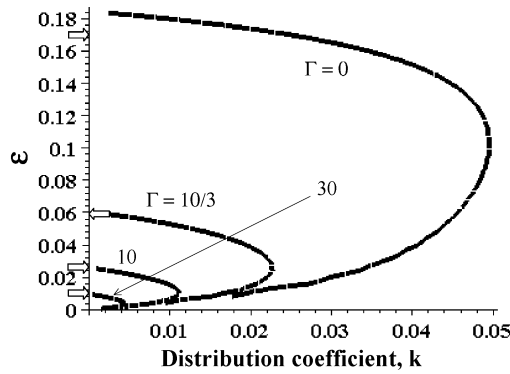


Fig. 9. Influence of the hydrostatic pressure parameter Γ on the dimensionless gap width versus the segregation coefficient k of the dissolved gas between the solid and the melt. \Leftrightarrow from the solution for material balance with $N_S^* = 0$, Eq. (25).

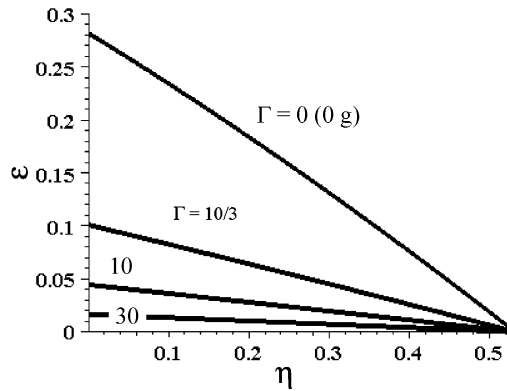


Fig. 10. Detachment with no dissolved gas entering the solid ($N_S = 0$). Dimensionless gap width ε versus meniscus parameter η for different values of dimensionless hydrostatic pressure Γ .

3.3. Material balance for finite gravity

We now consider detachment for non-zero acceleration a . For a 5 cm column of InSb at Earth’s gravity, we find $\Gamma = 31.5$. Figs. 9 and 10 show that for such a high value of Γ both steady-state gap widths are small and, furthermore, detachment is not possible unless the segregation coefficient k is small. However, in the foregoing we have assumed that there is no convective mixing in the melt. This is not realistic in the presence of acceleration.

4. Discussion

4.1. Influences of acceleration

We now consider other possible effects of acceleration on detachment. To do this, we examine the possible sinks for the dissolved gas:

Sink 1: It goes into the gap.

Sink 2: It goes into the solid.

Sink 3: It is liberated at the top free melt surface, either because convective mixing causes the flux into the domain at $x = L$ to become negative, or because the melt column above the freezing interface becomes shorter than the diffusion length D/V_c .

Sink 4: Gas bubbles nucleate and grow at the freezing interface [e.g. Ref. 9].

The first two of these have been considered here, with sink 1 maintaining the required pressure in the gap. All of these fluxes are influenced by acceleration. The required pressure in the gap is increased by the hydrostatic head, so that the flux into the gap must be increased for a given gap width. Sinks 3 and 4 reduce the amount of dissolved gas available to support detachment. The flux into the solid, sink 2, is influenced by the direction and strength of the adjacent convection in the melt. Convection directed inward toward the centerline of the ampoule carries rejected gas away from the gap, increases the concentration of dissolved gas along the freezing interface, and thereby increases sink 2. Convection directed radially outward toward the gap lowers the concentration, thereby reducing sink 2. The flux out of the top surface of the melt, sink 3, increases with increasing convection and decreasing melt height. As a result, one would not expect detachment of the last portion of the melt to solidify. The consequence of sinks 2 and 3 is that gentle outward convection increases the flux into the gap, while vigorous convection reduces it [6]. Thus, for example, a plot of flux into the gap versus a exhibits a maximum for outward convection, but a monotonic decline versus a for inward convection [6]. Since, for most materials, the convection is outward for a convex freezing interface, a slightly convex interface should aid detachment on earth.

In the absence of acceleration, gas bubbles that form at the freezing interface (sink 4) are incorporated in the growing solid, possibly in the form of tubes. With acceleration, nucleation of gas bubbles is made more difficult by the hydrostatic pressure, and may either be increased or decreased by convection, depending on whether the dissolved gas concentration is increased or decreased at the freezing interface.

Thus we see that a full theoretical treatment of detachment on earth would have to take into account convection in the melt. This treatment would introduce at least three additional dimensionless parameters for the melt: its Prandtl number, its Schmidt number, and the Grashof number or Rayleigh number.

Detached solidification has recently been observed on the ground using vertical Bridgman growth [10–19]. Detachment of Ge in a quartz ampoule was observed for 27 mm in one experiment in a transparent furnace [14]. The bottom 7 mm and the top 7 mm grew attached to the wall. A videotape of the ampoule during solidification showed the transitions from attachment to detachment and vice versa, along with the meniscus and the gap during detached growth [19]. Similar detachment was obtained here in several experiments on InSb using a quartz ampoule coated with pyrolytic boron nitride (PBN) and self-seeding [18], and at NASA's Marshall Space Flight Center on Ge using seeds in PBN crucibles closed on the bottom [15]. Reproducible detachment over a large length of GaSb was obtained by using a seed smaller in diameter than the ampoule combined with artificially maintaining the gas pressure in the gap either by using an external control [10] or by changing the temperatures in gas reservoirs at the two ends of the ampoule [11]. Similar results were obtained with CdTe [12] and for GeSi [16]. Duffar indicated that such a process is self-regulating because bubbles are emitted from the gap if the pressure exceeds that required [13].

4.2. Difference between material-balance solution and numerical solution

In the numerical solution, the velocity field is computed by solution of the Navier–Stokes equation and then used to solve the differential equation for component transport. The meniscus deflects the flow of melt toward the freezing interface away from the ampoule wall, causing an inward flow. This inward flow, which is completely neglected in the material-balance treatment, increases the concentration of dissolved gas along the freezing interface as one moves toward the centerline of the ampoule. This increases the calculated flux into the solid. Since this deflection increases with increasing gap width, the discrepancy between numerical and material-balance solutions increases with increasing gap width.

The influence of convection on component transport is determined by the Schmidt number, which is the ratio of the kinematic viscosity to the diffusion coefficient. In our previous numerical simulations for InSb, the kinematic viscosity was taken to be $3.6 \times 10^{-7} \text{ m}^2/\text{s}$, which yields a Schmidt number of 360. When the Schmidt number is much greater than 1, the concentration field is sensitive to the velocity field. Thus, it is gratifying that our material-balance solution nonetheless reveals the fundamental physics of detached solidification.

4.3. Stability

The relative stability of the two gap widths is of interest. By applying the Liapunov method to a numerical solution of the Moving Meniscus Model, the larger gap width was predicted to be more stable than the narrow one [5]. However, the physics was unclear. Let us use Fig. 3 to clarify the situation. Consider operation at the smaller gap width. If a perturbation causes the gap width to momentarily increase, the steady flux N_L^* into the domain exceeds that out ($N_S^* + N_G^*$). Since the solid cannot accommodate additional gas, the extra gas must flow into the gap and cause the gap width to increase still farther. Thus, the gas fluxes destabilize the small steady-state gap. On the other hand, for the larger steady-state gap a perturbation that increases the gap width leads to a decrease in gas flux into the gap and will return the gap to its steady value. Thus, the fluxes stabilize the large steady-state gap. It is interesting to note that microgravity experiments with very narrow gaps typically had small ridges contacting the ampoule wall [1], indicating that detachment with the meniscus completely surrounding the solid tended to be unstable. We have not yet considered this situation theoretically.

As shown in Ref. [5], capillarity destabilizes both wide and narrow gaps. Heat transfer, on the other hand, stabilizes both (as it does for Czochralski growth).

5. Conclusions

As illustrated in Fig. 3, this material-balance treatment captures the essential physics and reveals the reason for the existence of two possible steady-state gap widths for given experimental conditions. The flux into the domain decreases with increasing gap width, while the sum of the fluxes out exhibits a minimum. Thus there are two intersections where the overall material balance is satisfied.

The influences of all operating conditions and physical parameters on gap width were consolidated into five dimensionless parameters: the dimensionless meniscus factor η , the freezing rate Peclet number Pe , the interfacial segregation coefficient k for dissolved gas, the gas solubility ratio β between the end of the melt and the meniscus, and the ratio χ between the gas concentration in the gap and that in the melt adjacent to the meniscus.

Detachment on earth is possible, although more difficult than in space. The segregation coefficient for dissolved gas must be small. When detachment does occur, the gap width should be small.

Acknowledgements

This research was supported by NASA Grant NAG 8-1482. We are grateful to NASA's Marshall Space Flight Center for use of their supercomputer for the numerical solutions.

References

- [1] L.L. Regel, W.R. Wilcox, *Microgravity Sci. Technol.* 14 (1999) 152.
- [2] W.R. Wilcox, L.L. Regel, *Microgravity Sci. Technol.* 8 (1995) 56.
- [3] D.I. Popov, L.L. Regel, W.R. Wilcox, *J. Mater. Synth. Proc.* 5 (1997) 283.
- [4] Y. Wang, L.L. Regel, W.R. Wilcox, *J. Crystal Growth* 209 (2000) 175.
- [5] D.I. Popov, L.L. Regel, W.R. Wilcox, *J. Mater. Synth. Proc.* 5 (1997) 299.
- [6] D.I. Popov, L.L. Regel, W.R. Wilcox, *J. Mater. Synth. Proc.* 5 (1997) 313.
- [7] Y. Wang, L.L. Regel, W.R. Wilcox, *J. Crystal Growth* 226 (2001) 430.
- [8] T. Duffar, P. Boiton, P. Dusserre, J. Abadie, *J. Crystal Growth* 179 (1997) 397.
- [9] W.R. Wilcox, V.H.S. Kuo, *J. Crystal Growth* 19 (1973) 221.
- [10] T. Duffar, P. Dusserre, F. Picca, S. Lacroix, N. Giacometti, *J. Crystal Growth* 211 (2000) 434.
- [11] T. Duffar, P. Dusserre, N. Giacometti, *J. Crystal Growth* 223 (2001) 69.
- [12] T. Duffar, Private communication, Ecole Nationale Supérieure d'Hydraulique et de Mécanique de Grenoble, L'Institut Nationale Polytechnique de Grenoble, France, 2001.
- [13] T. Duffar, Private communication, Ecole Nationale Supérieure d'Hydraulique et de Mécanique de Grenoble, L'Institut Nationale Polytechnique de Grenoble, France, 2002.
- [14] P. Dold, F.R. Szofran, K.W. Benz, *J. Crystal Growth* 234 (2002) 91.
- [15] M. Schweizer, S.D. Cobb, M.P. Volz, J. Szoke, F.R. Szofran, *J. Crystal Growth* 235 (2002) 161.
- [16] M.P. Volz, M. Schweizer, N. Kaiser, S.D. Cobb, L. Vujisic, S. Motakef, F.R. Szofran, *J. Crystal Growth* 237–239 (2002) 1844.
- [17] M. Schweizer, M.P. Volz, S.D. Cobb, L. Vujisic, S. Motakef, J. Szoke, F.R. Szofran, *J. Crystal Growth* 237–239 (2002) 2107.
- [18] J. Wang, MS Thesis, Clarkson University, Potsdam, New York, 2002.
- [19] F. Szofran, P. Dold, Private communication, NASA Marshall Space Flight Center, Alabama, 1998.